Experiments in Fluids 9, 49–58 (1990)

Experiments in Fluids

Dynamic stall experiments on the NACA 23012 aerofoil

J. G. Leishman

Dept. of Aeronautics and Fluid Mechanics, University of Glasgow, Glasgow G12 8QQ, Scotland, UK

Abstract. An experimental investigation was conducted to examine the dynamic stall characteristics of a NACA 23012 aerofoil section at a Reynolds number of 1.5 million. Time-dependent data were obtained from thirty miniature pressure transducers and three hot film gauges situated at the mid-span of the wing. The static stall mechanism of the NACA 23012 was determined to be via abrupt upstream movement of trailing edge separation. Under dynamic conditions, stall was found to occur via leading edge separation, followed by a strong suction wave that moved across the aerofoil. This suction wave is characteristic of a strong moving vortex disturbance. Evidence of strong secondary vortex shedding was also found to occur, and this appears symptomatic of dynamic stall only at low Mach numbers. Some evidence of flow reversals over the trailing edge of the aerofoil were indicated prior to the development of leading edge separation and dynamic stall.

List of symbols

c	aerofoil chord
C_L	sectional lift coefficient
C_M	sectional pitching moment coefficient measured about the quarter-chord location
C_p	pressure coefficient
k	reduced frequency, $\omega c/2V$
M	Mach number
P	pressure
R_c	Reynolds number based on chord c
t	time
V	free stream velocity
x	distance along chord line
y	distance along span
α	angle of attack
α_a	oscillation amplitude
α_M	Mean angle of oscillation
τ	shear stress
ω	circular frequency

1 Introduction

Dynamic stall occurs on a lifting aerofoil when it is subjected to an increasing angle of attack, which subsequently exceeds the normal static stall angle at some significant pitch rate. During this process, the fluid mechanics of the stall are generally considerably different from those obtained on an aerofoil under static conditions. It has been observed that the flow remains attached to the aerofoil surface to angles of attack significantly higher than could be attained statically, with a corresponding increase in maximum lift. Kramer (1932) appears to have been one of the first investigators to recognise these dynamic lift effects on a pitching aerofoil.

When dynamic stall occurs, it is now well known that the fluid mechanics are characterised by the formation and shedding of a vortex-like disturbance from the leading edge region of the aerofoil. The passage of this vortex across the upper aerofoil surface induces a moving pressure wave which provides additional vortex lift. This vortex lift is also accompanied by significant increases in nose down pitching moment due to the redistribution of chordwise pressure. A qualitative understanding of this vortex shedding phenomenon was first given by Ham (1968). After the vortex disturbance passes the aerofoil trailing edge and into the wake, the flow progresses to a state of full separation over the upper surface. This is accompanied by a sudden loss of lift and decrease in pitching moment. If and when the angle of attack becomes low enough, the flow will finally reattach again from the leading edge. The general consequences of the flow physics on the lift and moment behaviour on an aerofoil undergoing dynamic stall are illustrated in Fig. 1.

Significant unsteady aerodynamic effects and dynamic stall are experienced on a variety of rotating machinery, at least over part of their operating range. Examples include rotors, wind turbines and compressors, all of which are discussed by McCroskey (1977). Probably the most well known form of dynamic stall is on a helicopter rotor (e.g. Young 1981), the consequences of which produce structural loads which severely limit the forward flight speed of the aircraft. Since most machinery is designed to avoid the operating conditions where stall effects appear, it is significant that more recently there has been interest in exploiting dynamic vortex lift on super-manoeuvrable aircraft (Lang 1985). Nevertheless, to utilise the potential of these energetic flows it is first necessary to both understand and predict the physics of the dynamic stall process across a wide range of operational parameters.

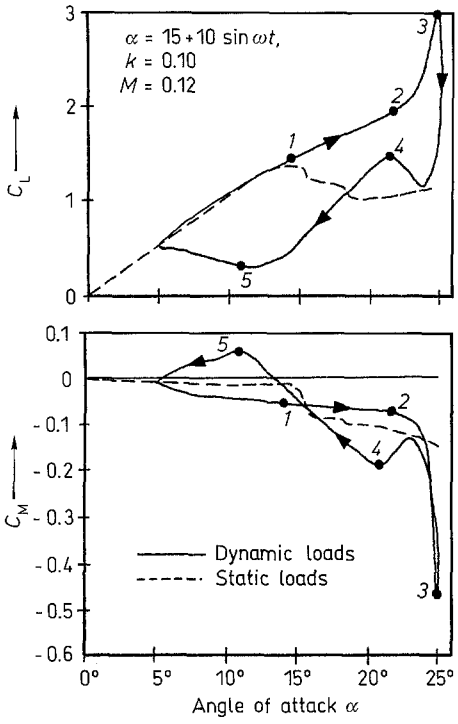

Fig. 1. Qualitative features of dynamic stall on an oscillating aerofoil [adapted from Carr (1977)]; *1* – static stall angle exceeded; *2* – leading edge vortex forms; *3* – vortex reaches trailing edge; *4* – secondary vortex reaches trailing edge; *5* – flow attachment begins

Theoretically, the phenomenon of dynamic stall has received considerable attention. However, because of the complexity of the phenomenon, early methods were semi-empirical based using significant input from experimental observations. These methods were often adequate for rotor design purposes, but lacked generality when applied to different aerofoils and different Mach numbers where test data was not always available. McCroskey (1981) concluded that all the theoretical methods available at that time were in need of dramatic improvement. Recently, computational fluid dynamics have shown some promise for predicting dynamic stall. Sankar and Tang (1985) have used the compressible, Reynolds averaged Navier Stokes equations for the computation of both laminar and turbulent flow fields about oscillating aerofoils. Although some success has been achieved with this method, predictions of the airloads in the post stall regime are still unsatisfactory. It is clear that because dynamic stall is characterized by massive recirculating separated flow regimes, proper theoretical simulation can only be achieved using the full Navier-Stokes equations with a suitable turbulence model.

Experimental investigations by numerous researchers have shown that dynamic stall is dependent on combinations of onset flow parameters and angle of attack forcing conditions. The characteristic leading edge vortex shedding phenomena has been well documented in the literature, e.g. Martin et al. (1974), McCroskey et al. (1976), Carr et al. (1977) and McAlister and Carr (1978). However, it appears that various degrees of vortex shedding phenomena may occur, depending primarily on the aerofoil motion and the extent to which stall is penetrated. Unfortunately, only a limited range of test conditions have been examined in detail thus far, and much experimental work still remains to be done before a thorough understanding of the phenomenon is obtained. This paucity of experimental data also hinders the continued development and validation of predictive methods.

The primary scope of this work was to experimentally investigate the two-dimensional unsteady aerodynamics and dynamic stall characteristics of a NACA 23012 aerofoil section at combinations of Reynolds number and Mach number typical of the retreating blade on a helicopter rotor. The NACA 23012 aerofoil is representative of current and projected helicopter rotor aerofoils, and while it has been tested before under static conditions, e.g. Abbott et al. (1945), Abbott and Doenhoff (1959), Althaus and Wortmann (1981), it has not been previously tested under unsteady conditions. The main objectives were to investigate the details of the stall mechanism and to more thoroughly document the influence of aerofoil motion on the onset of dynamic stall. A secondary aspect of the investigation was to obtain a comprehensive data base of unsteady aerodynamic data over an extensive matrix of test conditions to support the validation of theoretical modeling of the phenomenon. The present work provides added foundation for understanding the behaviour of separated flow on an aerofoil under unsteady conditions.

2 Test apparatus

The experiments were conducted in the Handley-Page low-speed wind tunnel at the University of Glasgow. This tunnel is an atmospheric pressure closed return type with a 1.61 by 2.13 m octagonal working section. Turbulence levels in the wind tunnel were measured with a hot wire anemometer and were found to be about 1.5% of the free-stream velocity. The NACA 23012 wing was mounted vertically to span the 1.61 m dimension of the wind tunnel. A wing chord of 0.55 m was selected based on maximising the chord Reynolds number whilst minimising blockage and wind tunnel interference effects. Labyrinthed end flanges were recessed flush with the tunnel walls and provided and airtight seal. The wing was constructed of a laminated mahogany and Tufnol profile mounted on a steel spar with a removable instrument section at mid-span. The aerofoil profile was machined to an accuracy of about ±0.3 mm and the surface wet sanded using No. 600 grit paper to ensure a smooth finish.

The wing was oscillated in angle of attack about the quarter chord axis by means of a hydraulic actuator and crank mechanism, as shown in Fig. 2. A precision angle of attack displacement transducer was incorporated into the system for angle of attack measurement and actuator feed-

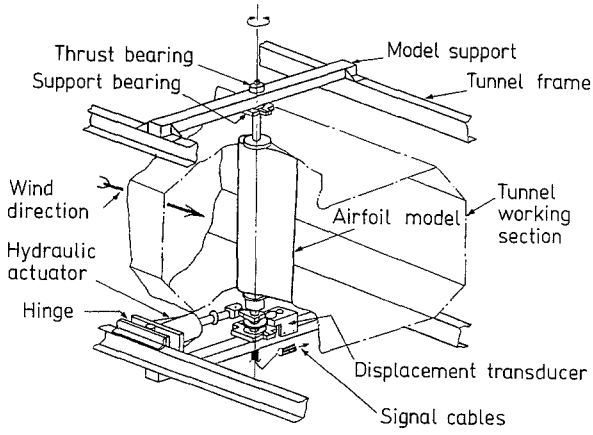

Fig. 2. General arrangement of the aerofoil and drive mechanism

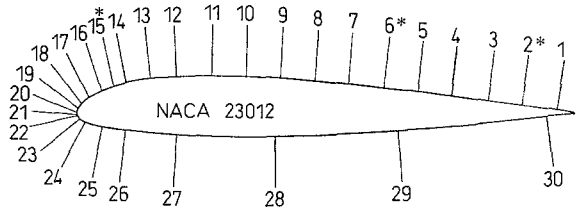

		Location x/c			
1	0.97	11	0.27	21	0.0 (upper)
2	0.90	12	0.20	22	0.0 (lower)
3	0.83	13	0.15	23	0.01
4	0.76	14	0.10	24	0.02
5	0.69	15	0.075	25	0.05
6	0.62	16	0.05	26	0.10
7	0.55	17	0.025	27	0.20
8	0.48	18	0.01	28	0.40
9	0.41	19	0.005	29	0.65
10	0.34	20	0.0005	30	0.95

Fig. 3. The NACA 23012 aerofoil showing the location of pressure transducers and hot films; * – hot film location

back control. Input signals to the actuator controller were provided by a digital to analog converter and a synthesised signal generator. Any combination of mean angle of attack, amplitude, and oscillation frequency could be set with the system. Fourier analysis showed that the pitch motion was almost a pure first harmonic; higher harmonics of the oscillation were measured to be less than $\pm 0.05\%$ of the fundamental.

3 Instrumentation

Data were obtained from 30 miniature Kulite and Entran pressure transducers which were located in a removable instrument section at the mid-span of the wing. Each transducer was of sealed-gauge construction with one side of the pressure diaphragm referenced to atmospheric pressure during manufacture. The locations of the transducers around the aerofoil are shown in Fig. 3. Each transducer was located in a machined slot immediately below a 1.0 mm orifice in the aerofoil surface and was sealed in place with RTV. The transducers were subjected to a static pressure test and calibrated against a quartz-gauge reference. Since the oscillating wing created a time-varying blockage in the tunnel, the instantaneous dynamic pressure in the wind tunnel was determined using a pitot-static probe connected to a fast response reference pressure transducer. This probe was situated approximately one chord length upstream of the leading edge of the aerofoil.

The instantaneous outputs from these pressure transducers, along with the instantaneous angle of attack, were interfaced to a thirty-two channel data acquisition system and then to a DEC MINC-11 (PDP 11/23) microcomputer for digitisation and subsequent processing. A 12 bit A/D converter was used. High gain amplifiers used in the system were band limited to 300 Hz, which was sufficient to pass the required signal bandwidth whilst minimising any aliasing errors associated with A/D sampling. To overcome time-skew errors associated with the multiplexed A/D system, a multi-channel sample and hold device was interfaced between the amplifiers and the MINC multiplexer.

The upper surface boundary layer characteristics were examined using a DISA constant temperature anemometry (CTA) system with DISA single filament film probes. Various technical problems with the system restricted the investigation to the use of three probes which were located adjacent the pressure locations at 7.5%, 62% and 90% chord (Fig. 3). No formal calibration was performed on the CTA system as the objective for these experiments was only to document the qualitative behaviour of the boundary layer shear stress characteristics. The outputs from the CTA system, simultaneously with the adjacent pressure transducer outputs, were recorded on photo sensitive paper using a UV beam galvanometer. Although only a few hot film sensors were used, they were found to aid significantly in the interpretation of the overall flow structure.

Considerable effort was taken to minimise sources of error in the experiments. Because of the relatively low signal outputs from the pressure transducers, efforts were made to maximise the signal to noise ratio. Transducer signal wires were composed of twisted pairs to maximise common mode rejection. Also, each pair of wires was individually shielded and connected to a common ground to minimise noise pick-up. By restricting tunnel run times and conducting frequent end-to-end checks of the zero offsets, the pressure coefficients could be reproduced to within ± 0.02 at a Reynolds number of 1.5 million. Corresponding errors in the lift and pitching moment coefficients were estimated to be less than $\pm 3\%$. The angle of attack was measured to an accuracy of $\pm 0.05°$ and the oscillation frequency to less than ± 0.0001 Hz. Further details are given by Leishman (1984).

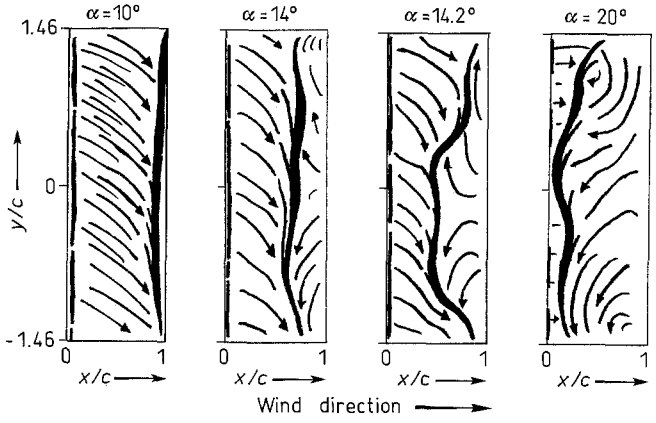

Fig. 4. Flow visualisation of stalled flow development under static conditions

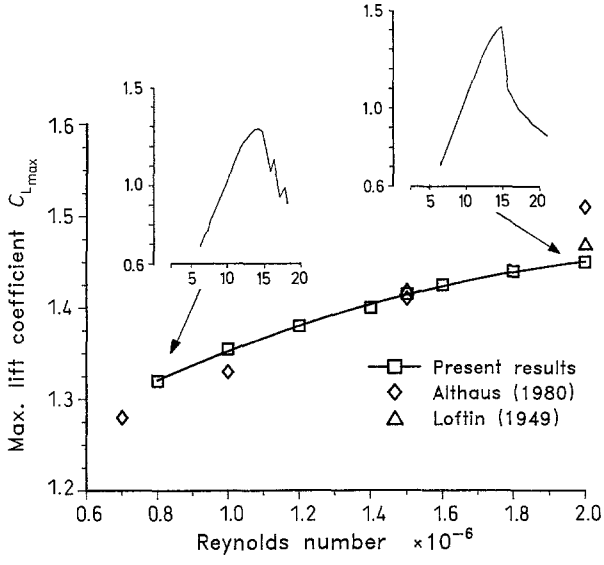

Fig. 5. Influence of Reynolds number on the static lift behaviour

4 Results and discussion

Prior to the unsteady tests, a series of static tests were made to determine the static stall characteristic of the aerofoil. As shown by Gault (1956), the NACA 23012 normally falls into the classification of a combined leading edge/trailing edge stall mechanism. Oil flow visualisation tests were also conducted to assess the three-dimensional flow development over the wing. Moss and Murdin (1968) have shown that two-dimensional flow is extremely difficult to attain on any wing configuration with any aspect ratio, especially near maximum lift. Under these conditions, the flow generally separates in a non-uniform manner across the span and forms a series of "stall cells". Although in the present experiment the pressures were measured at the mid-span where three-dimensional effects are generally much less, it was nevertheless important to have some knowledge of the stalled flow pattern on the wing.

Odina oil containing a fluorescent compound was applied to the aerofoil and illuminated under UV-B light. The wind tunnel was set to the required speed followed by setting the wing to the desired angle of attack. Photographs were taken of the resulting flow patterns for various angles of attack up through stall. Sketches were made from the photographs for clarity and a selected sample are presented in Fig. 4 for a Reynolds number of 1.5 million. It should be noted that since the wing was mounted vertically in the tunnel there is a downward bias to the oil flow patterns due to gravity. Accumulations of oil formed in regions of low surface shear and are indicated by the dark bands in Fig. 4.

Up to an angle of attack of 12°, the flow was found to be fairly two-dimensional with little or no separation on the aerofoil, except at the very trailing edge. A characteristic "scarf" vortex was also noticed at the wing/tunnel wall juncture, and this appeared to significantly help keep the flow attached to the aerofoil in these regions. Transition from a laminar to a turbulent boundary layer was clearly shown via a separation bubble which became narrower and moved closer to the leading edge with increasing angle of attack. This can be seen in the sketches in Fig. 4 as a narrow dark band at about 3%–5% chord. The presence of the bubble sometimes appeared irregular because of a local accumulation of oil.

At 14° angle of attack, trailing edge separation began to increase in a somewhat nonuniform manner across the span. At an angle of 14.2°, the separation front moved very quickly to the leading edge with indications of trailing vortices forming in an asymmetric manner at the outer span regions. The laminar separation bubble remained present during this process, confirming that stall was not due to laminar separation bubble bursting. With further increases in angle of attack, the trailing vortices appeared to grow somewhat stronger and then weaker at about 20° when massive flow separation was obtained over the whole of the upper surface. Significant portions of the laminar separation bubble also remained present in the leading edge region up to this high angle of attack. The qualitative features of the three-dimensional static stall development were similar at all the Reynolds numbers tested. Further details are given by Seto et al. (1983).

Static pressure data were obtained over an angle of attack range from −4° to 28° and at Reynolds numbers between 0.8 and 2.0 million. These static tests were conducted by changing the angle of attack in increments of 0.5°, followed by ensemble averaging the pressure transducer outputs on each channel over a 5 s period. After reaching a maximum angle of attack of about 30°, the procedure was repeated by decrementing the angle of attack until the aerofoil was returned to its original position. Some weak flow hysteresis was found between the upgoing and downgoing motions.

The influence of Reynolds number of the maximum static lift coefficient is shown in Fig. 5. Reynolds number was found to have a moderately large influence on the maximum lift coefficient and also on the stall characteristic itself (in-

sets), which became more abrupt with increasing Reynolds number. As determined by Loftin and Hamilton (1949) and Gault (1956), the NACA 23012 aerofoil should fall into the leading edge or bubble bursting stall category because of the abrupt stall at higher Reynolds numbers. However, careful examination of the pressure time histories and hot film records along with the flow visualisation results confirmed the static stall mechanism to be via the abrupt upstream movement of trailing edge separation. The static data in Fig. 5 are also compared with measurements made by Loftin and Hamilton (1949) and Althaus and Wortmann (1981) in a very low turbulence wind tunnel. The results were in good agreement and give considerable confidence to the measurements made here.

Although the static tests described above are of some interest and value, it must be remembered that in the environment of a helicopter rotor the stall is actually dynamic in nature. Thus, the static stall mechanism and the maximum static left are not necessarily reliable indicators as to how the aerofoil will perform at high angles of attack under unsteady conditions. Other criteria, such as the attainment of high lift with a low pitching moment, become more important indicators of the aerofoil's performance for helicopter applications. To this end, the main objective of this experiment was to explore the unsteady behaviour of the NACA 23012 aerofoil and to establish how its performance would change under different combinations of oscillatory forcing. Many of these conditions were selected to be typical of the angle of attack time history that a blade section would encounter on a helicopter rotor in forward flight. Oscillatory pressure data were recorded for over 500 test conditions and consisted of systematic variations of mean angle of attack α_M, oscillation amplitude α_a, and chord Reynolds number R_c. Data were obtained at reduced frequencies k (based on semi-chord) of 0.01, 0.05, 0.10, 0.15 and 0.20.

Contrary to the static stall characteristics, the dynamic tail characteristics of this aerofoil were found to be only weakly dependent on Reynolds number, and the following data in this paper refers to these recorded at a Reynolds number of 1.5 million. 128 data points from each of the pressure sensors were recorded during each pitch cycle. Data from ten pitch cycles were then ensemble averaged. The lift and pitching moment about the quarter-chord were obtained by numerically integrating the pressure distribution across the chord.

4.1 Effect of mean angle of attack

Figure 6 shows the effects on the lift and moment by increasing the mean angle of attack of the oscillation from 6° to 20° at a constant oscillation amplitude of 10° and reduced frequency of 0.1. The static behaviour is shown by the broken line in each figure. At the lowest mean angle, the flow is almost fully attached to the aerofoil and characteristic elliptical lift and moment loops are obtained. This is indicative of unsteady potential flow and can be well predicted using linearised methods (Bisplinghoff et al. 1955). As the mean angle is increased to 12°, dynamic stall is obtained, with high values of lift and moment along with significant hysteresis. It should be noted that on the downstroke of the motion the angle of attack falls to almost 4° before the lift and moment return to their "attached" flow values. This indicates the adverse effect of a negative pitch rate which delays the flow reattachment process. Also, under these conditions the aerodynamic pitch damping $-\oint C_M \, d\alpha$ was negative indicating that this situation may be a source of aeroelastic instability on a helicopter rotor or wind turbine [1].

At the highest mean angle of 20°, even larger lift and nose down moment coefficients were obtained. Maximum lift coefficients were nearly 100% higher than those obtained under static conditions. Also, there were large non-linear changes to the lift curve slope just prior to maximum lift. This condition vividly illustrates the delay between break in the pitching moment and the occurrence of maximum lift. The moment break (or stall) occurs at about 20° angle of attack, whereas the lift stall occurs at about 25°. It is significant to note in Fig. 6, the appearance of large secondary peaks in the lift and moment near the maximum angle of attack. It is likely that these secondary peaks may be due to the formation and convection of another vortex across the chord. Again, as in the previous case, there is a considerable delay in flow reattachment during the downstroke of the motion.

The time history of the chordwise pressure distribution on the aerofoil is shown in Fig. 7 for one cycle of the aerofoil motion. It is significant that the flow remains nominally attached to the aerofoil up to an angle of attack of about 21°. It is also worthy to note the unusually high leading edge suction peaks that are attained on the aerofoil, i.e. pressure coefficients of −14. Under static conditions, the minimum static C_p at the leading edge is about −7.5. This clearly illustrates the favourable effects of a positive pitch rate in keeping the boundary layer attached to the aerofoil to much higher angles of attack than could be attained under static conditions.

The corresponding increase in adverse pressure gradient also makes the aerofoil more susceptible to leading-edge separation. It appears that this is indeed the case here, since the leading edge pressures collapse at about 21° angle of attack but without any significant divergence in the trailing edge pressures. The pressure signature made by the primary vortex can be readily observed in Fig. 7 near 25% chord at about 22°–24° angle of attack. As the vortex moves over the chord, the trailing edge pressures progressively diverge. After the primary vortex reaches the trailing edge (about 28°), the pressures collapse whilst simultaneously another, although somewhat weaker, moving pressure wave develops near 25% chord and convects more quickly over the chord. It is interesting that the strong secondary pressure waves observed in this experiment appear characteristic of dynamic stall only at low Mach numbers and do not appear to be

1 Negative damping is indicated by a clockwise moment loop

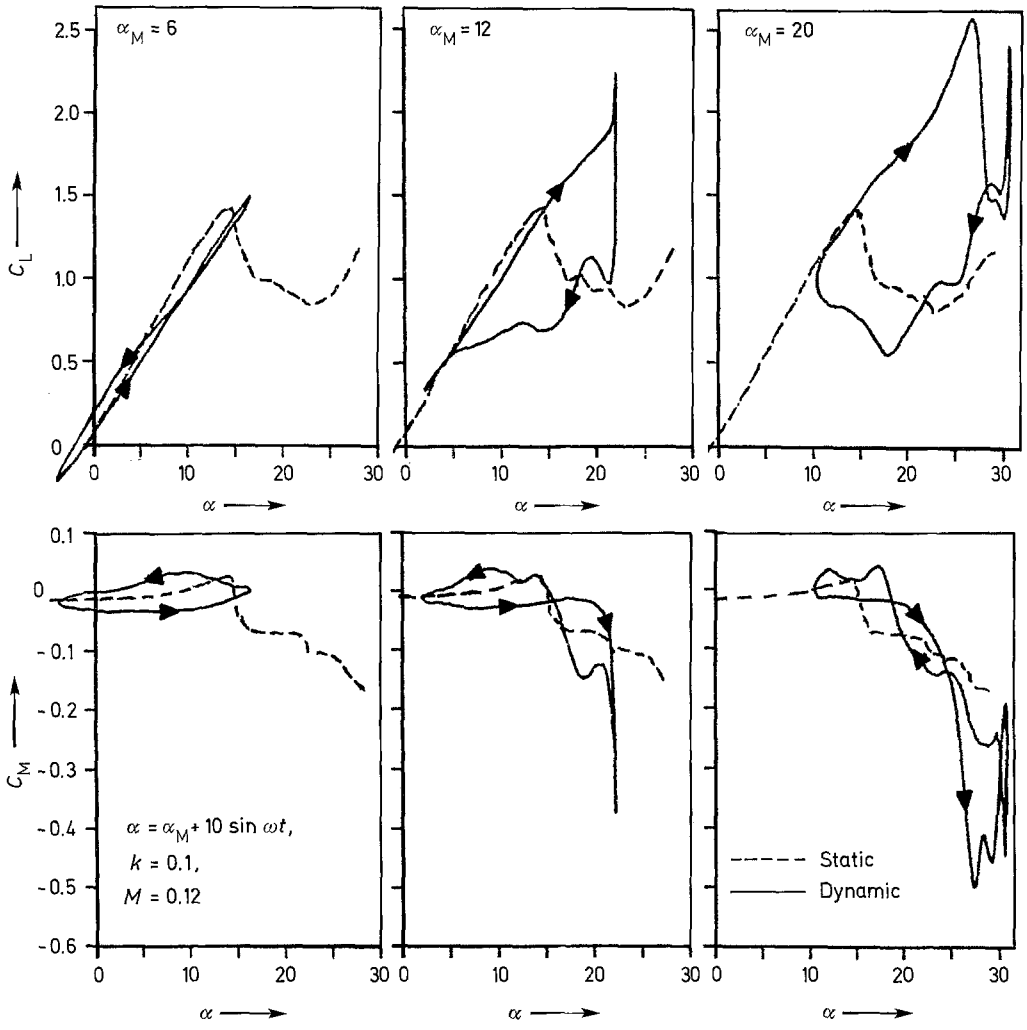

Fig. 6. Effects on the unsteady lift and moment for variations in mean angle of attack

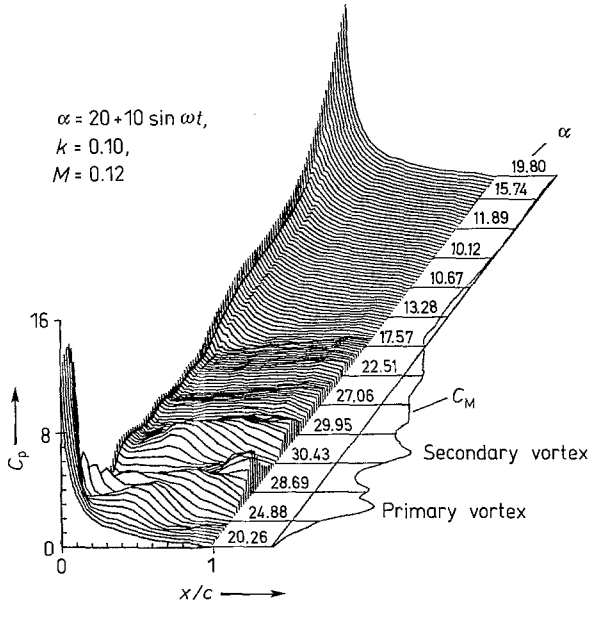

Fig. 7. Chordwise pressure time histories showing the vortex induced pressure loading during dynamic stall

present (not, at least, to the same degree) for dynamic stall at Mach numbers above 0.3 (e.g. Woods 1979). After the secondary vortex has passed the trailing edge, the pressures remain fairly uniform across the chord indicating that the flow has completely separated from the upper surface. At about 17° angle of attack, the flow begins to reattach to the aerofoil (front to back) and the normal form of the chordwise pressure distribution is finally obtained for angles of attack below the normal static stall angle. During this reattachment process, some evidence of the laminar separation bubble can be seen by the "flat spot" in the pressure distribution near 10% of chord.

4.2 Effect of oscillation amplitude

The effects on the lift and moment by increasing the oscillation amplitude at a constant mean angle of 18° and reduced frequency of 0.15 are shown in Fig. 8. At the lowest amplitude of 2°, the aerofoil is completely stalled, however some limited hysteresis was still apparent. At an amplitude of 6°, the characteristic dynamic stall loops re-appear. It is inter-

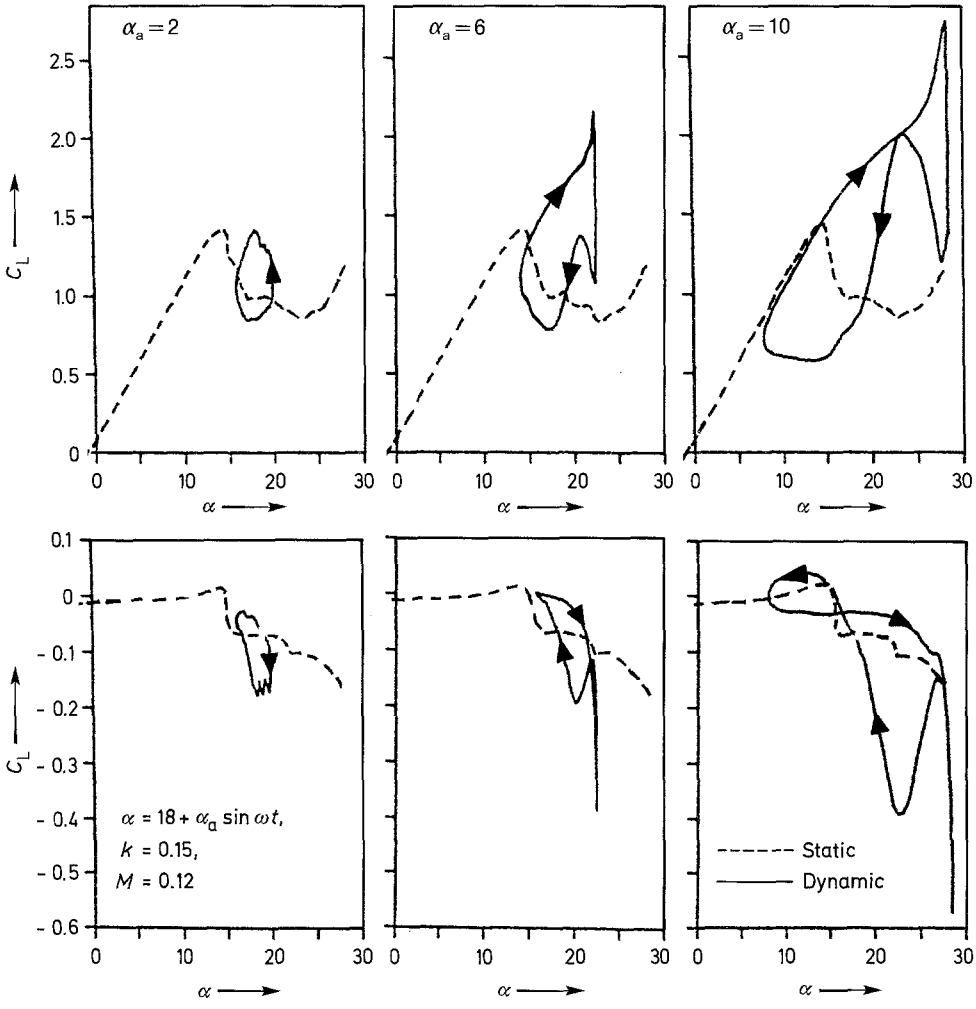

Fig. 8. Effects on the unsteady lift and moment for variations in oscillation amplitude

esting that significant dynamic lift gains are experienced for this case, even though the aerofoil is still operating essentially above the normal static stall angle of attack. Examination of the pressure time histories (not shown) indicated that the amplitude of the motion was just sufficient to cause flow reattachment at the lowest point in the cycle, after which the favourable pressure gradients induced by the positive pitch rate kept the flow attached until dynamic stall was finally obtained.

At the highest amplitude of 10°, extremely large primary lift and moment peaks were obtained accompanied again by very strong secondary peaks on the downstroke of the motion. In this case, the onset of secondary vortex shedding does not occur until the downstroke of the motion is well established. This is partially because the aerofoil is oscillating at a higher frequency, so the event occurs at a later point in the pitch cycle. It is important to note, that at this high mean angle of attack the aerodynamic pitch damping is strongly negative, i.e. a large clockwise moment loop. For an aeroelastic system such as a wing or helicopter rotor blade, this is another flow regime that could result in a torsional instability.

4.3 Effect of reduced frequency

Of the parameters varied in this experiment, the reduced frequency of the oscillation was found to be highly significant. Figure 9 shows the effects of increasing reduced frequency at a mean angle of 10° at a constant amplitude of 10°. At the lowest frequency of 0.1, the characteristic dynamic stall loops are obtained, as before. As the frequency was increased to 0.16 and then to 0.20, it can be seen that the loops become much narrower with significantly less hysteresis. At the same time, the peak pitching moment coefficient drops significantly from about -0.35 to -0.08.

It is apparent from these figures, that the initial effects of increasing reduced frequency (or increasing pitch rate) are to delay the onset of flow separation and dynamic stall to a higher angle of attack. In fact, it was found that only small values of reduced frequency (or positive pitch rate) were required to significantly delay the onset of stall. Furthermore if the frequency is sufficiently high then it appears that flow separation does not have time to develop. Under these conditions, the onset of stall occurs at the maximum angle of attack in the pitch cycle and is induced by a highly adverse

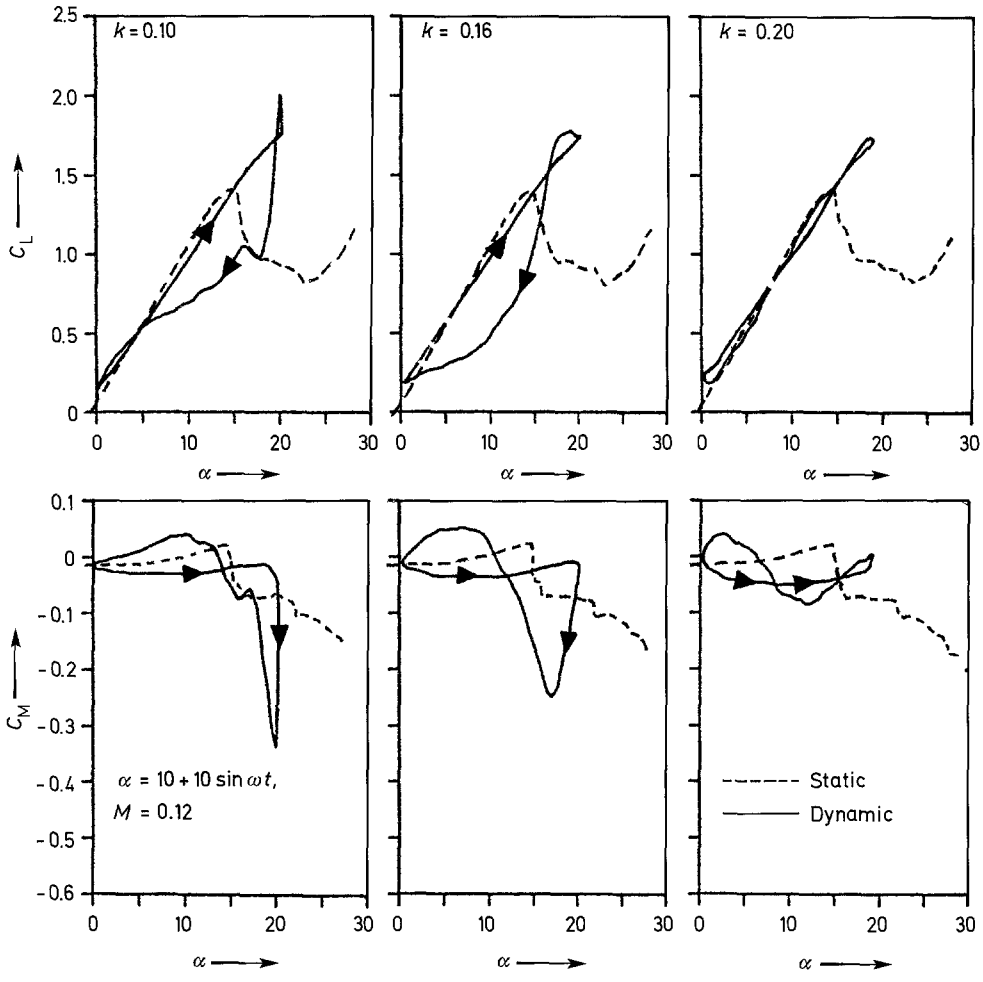

Fig. 9. Effects on the unsteady lift and moment for variations in reduced frequency

leading edge pressure gradient coupled with a diminishing positive pitch rate.

4.4 Hot film data

To help understand the complex behaviour of the flow during the dynamic stall process, three hot films were located on the aerofoil. The outputs were uncalibrated and provided only a qualitative representation of the boundary layer shear stress behaviour. A typical set of shear stress time histories, along with the corresponding pressures, are shown in Fig. 10 and have been traced from the original analog record. The repeatability from cycle to cycle was found to extremely good, and only one cycle need be shown. It should be noted that all values are unscaled but each set of the pressure and hot film output channels have nominally the same sensitivity and thus can be compared directly in magnitude. The particular data in Fig. 10 correspond to the lift and moment results given previously in Fig. 6.

As the angle of attack increases, the film gauge at 7.5% chord ($\tau_{0.075}$) was the first sensor to show a significant change in output with a sudden increase at point 1. This corresponds to the forward movement of laminar to turbulent boundary layer transition point across the gauge. With a further increase in α, the pressures at all the locations showed a monotonic decrease in output corresponding to the development of suction on the aerofoil upper surface. The mean value from the film gauges at 62% and 90% chord also showed a progressive reduction in output over this α range. It should be noted that gauge fluctuations increased significantly from the leading edge to the trailing edge gauge indicating the increasing turbulence fluctuations in the boundary layer.

At point 2, the pressure at 7.5% chord ($P_{0.075}$) shows a sudden decrease in output due to the loss of leading edge suction followed a short time later by sharp transient (point 3) as the pressure instantaneously regained a value close to that which would have been attained if suction had not been lost at point 2. This was not a spurious transient and was repeatable from cycle to cycle. The corresponding film gauge showed a drop in output at point 2 followed by a sharp increase at point 3 and then a decrease again. From this behaviour, it appears that the dynamic stall vortex forms downstream of 7.5% chord and as it breaks from the aerofoil surface it induces a flowfield which instantaneously reduces the angle of attack at the leading edge thereby permitting the re-establishment of laminar flow at least as far as 7.5% chord.

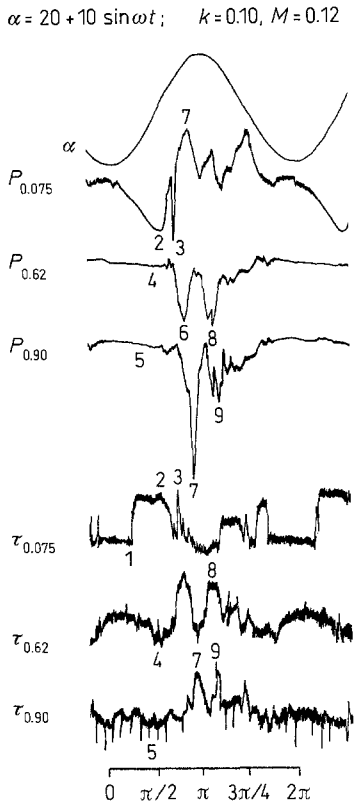

Fig. 10. Typical time histories of hot film and corresponding pressure responses

All the other film sensors showed a sudden change in output either slightly before or after the loss of suction at point 2, indicating a gross change in the flow structure about the aerofoil. Referring to the sensor at 62% chord, it can be seen that minimum in the shear stress is obtained (point 4) without any notable change in the corresponding pressure. This type of minimum obtained with a single filament hot film gauge is indicative of a change in the flow direction. In the absence of any pressure change at point 4, it is likely from these results that flow reversals may be taking place within the boundary layer in the absence of any significant flow separation. A similar result may be concluded from the behaviour of the sensors at 90% chord, with a minimum shear stress being attained near point 5, i.e. just prior to point 4. It is significant that these flow reversals occur before the loss of leading edge suction at point 2, and hence before the onset of leading edge separation.

Immediately after point 2, the pressures at both 62% and 90% chord show a slight increase in output followed by sharp decrease, as marked at points 6 and 7 respectively. These pressure peaks correspond to the passage of the vortex across the chord during dynamic stall. Using the difference in time between points 6 and 7, the pressure wave convection velocity was determined to be approximately half the free-stream velocity which confirms the results of Carr et al. (1977). Analysis of other test conditions showed that this wave velocity was largely independent of mean angle, reduced frequency etc. Coinciding with points 6 and 7, the respective hot film gauges showed a peak in the output indicating that extremely high tangential velocities were induced on the aerofoil by the convecting vortex.

After the passage of the primary vortex, a series of smaller secondary peaks were obtained in the pressure responses indicating the passage of a weaker secondary vortex (points 8 and 9). This vortex was estimated to be less than half the strength of the primary vortex and traversed the chord at about 60%–70% of the free-stream velocity. After this, the angle of attack is decreasing rapidly and all the sensors show rapidly fluctuating outputs. This is consistent with the development of a large recirculating wake region over the upper airfoil surface. It is not until the aerofoil has reached the lowest angle of attack in the cycle (10°) that the sensors become more quiescent indicating that the flow has fully reattached to the aerofoil.

5 Conclusions

A series of experiments has been conducted to examine both the static and dynamic stall characteristics of the NACA 23012 aerofoil. Static stall of the aerofoil occurred by the mechanism of abrupt upstream movement of trailing edge separation at all the Reynolds numbers tested. The static stall abruptness was found to increase with increasing Reynolds number. Despite the fact that the aerofoil exhibited abrupt trailing edge stall under static conditions, under dynamic conditions separation always originated in the vicinity of the aerofoil leading edge. It appeared that only very low oscillation frequencies were required to suppress any trailing edge separation present, and convert the stall mechanism to a leading edge type stall stall. Thus, the static stall mechanism appeared largely irrelevant to the dynamic stall behaviour.

Overall, the dynamic stall characteristics of the aerofoil were found to be qualitatively similar to the characteristics of other aerofoils measured previously by other investigators. This included the large increments in lift and pitching moment coefficient which are induced by the shedding of a vortex disturbance from the leading edge region of the aerofoil during dynamic stall. The occurrence of significant secondary loading peaks were also found in this study and have been attributed to secondary vortex shedding. Strong secondary vortex shedding appears symptomatic only of dynamic stall at low Mach numbers. Boundary layer measurements performed using hot films indicated that surface flow reversals may have been present on the aerofoil just prior to the onset of any significant flow separation from either the leading edge or trailing edge of the aerofoil.

Further measurements are required to more fully explain the actual mechanism of dynamic stall onset, particularly

the nature of the flow within the scale of the boundary layer. However, it is significant that a positive pitch rate provides a beneficial effect and helps to keep the boundary layer attached to very much higher angles of attack over those which could be obtained statically. The accompanying high adverse leading-edge pressure gradients make the aerofoil more succeptable to leading-edge separation. Thus, it is clear that the static stall characteristics, such as stall type or maximum lift coefficient, are not necessarily useful indicators as to how an aerofoil will behave under dynamic stall conditions.

Acknowledgements

This work was supported by the U.K. Science and Engineering Research Council (SERC) and Westland Helicopters Ltd. under SERC CASE Studentship 80513408. Additional support was provided by the Royal Aircraft Establishment under MOD agreement 2084/026XR/STR. The author is indebted to his adviser, Dr. R. A. McD. Galbraith, for his advice and unfailing support during the course of this work.

References

Abbott, I. H.; Doenhoff, A. E. von 1959: Theory of wing sections including a summary of airfoil data. New York: Dover

Abbott, I. H.; Doenhoff, A. E. von; Stivers, L. S. 1945: A summary of airfoil data. NACA Report No. 824

Althaus, D.; Wortmann, F. X. 1981: Stuttgarter Profilkatalog 1. Experimental results from the laminar wind tunnel of the Institut für Aero und Gasdynamik der Universität Stuttgart. Braunschweig: Vieweg

Bisplinghoff, R. L.; Ashley, H.; Halfman, R. L. 1955: Aeroelasticity. Addison-Wesley, Cambridge/MA

Carr, L. W.; McAlister, K. W.; McCroskey, W. J. 1977: Analysis of the development of dynamic stall based on oscillating airfoil experiments. NASA TN D-8382

Gault, D. E. 1956: A correlation of low speed airfoil section stalling with Reynolds number and airfoil geometry. NACA TN 3956

Ham, N. D. 1968: Aerodynamic loading on a two-dimensional airfoil during dynamic stall. AIAA J. 6, 1927–1939

Kramer, M. 1932: Increase in the maximum lift of an airfoil due to a sudden increase in its effective angle of attack resulting from a gust. NASA Tech. Memorandum 678

Lang, J. D. 1985: Unsteady aerodynamics and dynamic aircraft maneuverability. AGARD CP 386. Unsteady aerodynamics – fundamentals and applications to aircraft dynamics, Göttingen, Paper No. 29

Leishman, J. G. 1984: Contributions to the experimental investigation and analysis of aerofoil dynamic stall. Ph.D. thesis. Department of Aeronautics and Fluid Mechanics, University of Glasgow

Loftin, L. K.; Hamilton, A. S. 1949: Aerodynamic characteristics of 15 NACA airfoil sections at 7 Reynolds numbers from 0.7 to 9.0 million. NACA TN 1945

Martin, J. M.; Empey, R. W.; McCroskey, W. J.; Carradonna, F. X. 1974: An experimental analysis of dynamic stall on an oscillating airfoil. J. Am. Helicopter Soc. 19, 26–32

McAlister, K. W.; Carr, L. W. 1977: Water tunnel experiments on an oscillating airfoil at $Re = 21{,}000$. NASA TM-78446

McCroskey, W. J. 1977: Some current research in unsteady fluid dynamics. The 1976 Freeman scholar lecture. J. Fluids Eng. 99, 8–38

McCroskey, W. J. 1981: The phenomenon of dynamic stall. NASA TM-81264

McCroskey, W. J.; McAlister, K. W.; Carr, L. W. 1976: Dynamic stall experiments on oscillating airfoils. AIAA J. 14, 57–63

Moss, G. F.; Murdin, P. M. 1968: Two-dimensional low speed tunnel tests on the NACA 0012 section including measurements made during pitching oscillations at the stall. British ARC CP 1145

Sankar, N. L.; Tang, W. 1985: Numerical solution of unsteady viscous flow past rotor sections. AIAA Paper 85-0129

Seto, L. Y.; Leishman, J. G.; Galbraith, R. A. McD. 1983: An investigation of three-dimensional stall developments on NACA 0012 and NACA 23012 aerofoils. University of Glasgow, Report GU-AERO-8300

Woods, M. E. 1979: Results from oscillatory pitch tests on the NACA 0012 blade section. Aircraft Research Association, Bedford. Memo 220

Young, W. H. Jr. 1981: Fluid mechanic mechanisms in the stall process of airfoils for helicopters. NASA TM 81956

Received August 22, 1989